Journal of Applied Electrochemistry **30**: 55–60, 2000.

Surface microstructure and corrosion resistance of electrodeposited ternary Zn–Ni–Co alloy

M.M. YOUNAN
Chemical Engineering and Pilot Plant Department, National Research Centre, Dokki, Giza, Egypt

Received 26 January 1999; accepted in revised form 15 June 1999

Key words: corrosion resistance, surface microstructure, ternary Zn–Ni–Co alloy

Abstract

The electroplating of ternary Zn–Ni–Co alloy, the influence of cobalt codeposition on crystal orientation, surface topography and corrosion resistance were investigated and contrasted with the characteristics of Zn–Ni electrodeposits. It was found that the Zn–Ni–Co alloy showed better corrosion resistance, in 3% sodium chloride, in comparison with Zn–Ni alloy electroplated under similar conditions. The best corrosion resistance was observed for ternary deposits having 11.24% Ni and 6.52% Co. The crystal orientation and surface topography were characterized by means of X-ray diffraction analysis and scanning electron microscopy, respectively.

1. Introduction

Extensive attempts have been made to develop highly corrosion resistance steel sheets, especially for the automotive industries [1–5]. It has been found that zinc–iron group metal alloy electrodeposits are suitable coatings for such applications [4–8]. A major development in this area has been directed towards zinc–nickel (8–20%) alloy coatings because of their high corrosion resistance and better physical properties in comparison with pure zinc layers [5, 7, 9]. However, the binary Zn–Ni thin films, in this range of nickel content, have a dull, grey, unattractive finish, and a brightener system must be developed to obtain bright deposits [10]. Suitable organic brighteners were developed to produce bright Zn–Ni electrodeposits [6, 7, 11]. Tsuda and Kurimoto [12] found that adding at least 0.05 g dm^{-3} $SrSO_4$ to Zn–Ni plating baths produced bright deposits. An upper concentration limit of 10 g dm^{-3} of $SrSO_4$ was required to prevent $SrSO_4$ precipitates.

Zn–Ni alloys exist in various phases and it is well known that the structure and morphology also determine the corrosion resistance of a deposit [13, 14]. Hall [9] emphasized that Zn–Ni alloy deposits are generally of anomalous type according to Brenner's definition [15]. Moreover, (i) there are important differences between the phase limits observed in electrochemically produced deposits and those of thermally prepared Zn–Ni alloys; (ii) the β phase has never been identified in the electrodeposits; (iii) the γ phase, identified in the deposits containing 12–14% nickel content, provides the best corrosion resistance. Elkhatabi et al. [16] found that the diffractograms of electrodeposited Zn–Ni (15–20%), always corresponded to the γ phase, with a (3 3 0) preferential orientation.

Recently, Younan and Oki [17] developed an acidic chloride bath with three separate anodes for the electrodeposition of bright ternary Zn–Ni–Fe alloy thin films, also with nonorganic brighteners. It was found that the Fe codeposition with Zn–Ni (14–19%) produces a clear change in the γ phase from (4 1 1) and (3 3 0) to a preferred (4 4 2), (6 0 0) or (4 4 4) crystal orientation [18]. These ternary Zn–Ni–Fe alloy coatings also exhibited better corrosion resistance and finer grain size in contrast to Zn–Ni deposits as reported by Oki and Younan [19].

The present work was carried out to study the crystal orientation, surface topography and corrosion resistance of ternary Zn–Ni–Co alloy deposits. Binary Zn–Ni and ternary Zn–Ni–Co deposits were obtained on mild steel plates by electrodeposition in a chloride bath. In order to make a clear comparison between Zn–Ni and Zn–Ni–Co alloys for crystal orientation, surface topography and corrosion resistance, the ternary alloys were prepared under similar electrolysis conditions to the binary Zn–Ni alloy.

2. Experimental details

The plating solutions were freshly prepared from distilled water and analytical grade reagents. The electrodeposition process was usually performed on mild steel plates at pH 3 $\pm$ 0.05, 30 mA cm^{-2} and 40 $\pm$ 2 °C for 10 min. The ternary Zn–Ni–Co and binary Zn–Ni alloys were electrodeposited from the basic bath given in Table 1 with and without cobalt chloride.

Table 1. Basic bath composition of ternary Zn–Ni–Co alloy electrodeposition

Bath composition	Concentration/M
Zinc chloride ($ZnCl_2$)	0.40
Nickel chloride ($NiCl_2.6\,H_2O$)	0.40
Cobalt chloride ($CoCl_2.6\,H_2O$)	0.08
Sodium chloride (NaCl)	2.50
Sodium acetate ($CH_3COONa.3\,H_2O$)	0.30
Boric acid (H_3BO_3)	0.50
Dodecyl sodium sulfate (wetting agent)	0.50*

* This concentration was in g dm^{-3}

A rectangular glass cell containing 200 cm^3 of electrolyte solution was used with a suitable electric circuit. Only one side of the steel samples (30 mm × 30 mm × 1 mm) was used as cathode, while pure zinc and nickel sheets (with areas 7.5 and 1.5 cm^2, respectively) were used separately as anodes. Two separate circuits fed by a d.c. power source regulated the anodic dissolution, where 86% of the total current was supplied through the zinc anode, and 14% through the nickel anode, in order to compensate the cathodic consumption of zinc and nickel. Before the electrodeposition process, the samples were pretreated as follows: degreasing by organic solvent (acetone), water rinsing, alkaline soaking in 6% NaOH, water rinsing, neutralization and activation for 60 s in 10% (v/v) HCl and finally rinsing with distilled water.

A pure copper substrate was used in the experiments for determination of the deposit composition; the deposits were then stripped in 10% (v/v) HCl solution and analysed by means of atomic absorption spectrophotometry. The crystal orientation was characterized by X-ray diffraction using Cu$K\alpha$ radiation ($\lambda = 0.154$ nm). The surface topography of the deposits was examined by means of scanning electron microscopy (SEM).

The samples for aqueous corrosion testing were mounted in an electrode holder of area 1 cm^2 exposed to the corrosion electrolyte. The corrosion currents and potentials for the different deposits were measured by the potentiodynamic polarization technique using a scanning potentiostat connected to a recorder. The corrosion experiments were performed in a conventional three-electrode cell containing 3% analytical grade sodium chloride at 23–25 °C at 5 mV s^{-1} scan rate. The potential was measured against a saturated calomel electrode (SCE), while the counter electrode was a platinum wire.

3. Results and discussion

3.1. *Deposit composition*

The electrodeposition of Zn–Ni–Co and Zn–Ni alloy coatings was carried out with constant parameters (30 mA cm^{-2}, 40 °C and pH 3 for 10 min) using the basic bath composition (Table 1) with varying Zn^{2+}/Ni^{2+} molar ratio in the presence and absence of Co^{2+}. Deposit compositions are given in Table 2.

Table 2. Effect of metal ion concentration in the bath on the deposit composition

Run	Metals ion concentration/M			Deposit composition/%		
	Zn^{2+}	Ni^{2+}	Co^{2+}	Zn	Ni	Co
1 (i)	0.5	0.4	0.00	86.93	13.07	00.00
(ii)	0.5	0.4	0.04	85.28	12.48	02.24
(iii)	0.5	0.4	0.06	84.19	11.93	03.88
(iv)	0.5	0.4	0.08	83.53	11.23	05.24
(v)	0.5	0.4	0.10	83.31	10.75	05.94
2 (i)	0.4	0.4	0.00	84.66	15.34	00.00
(ii)	0.4	0.4	0.04	82.96	13.78	03.26
(iii)	0.4	0.4	0.06	82.47	12.37	05.16
(iv)	0.4	0.4	0.08	82.24	11.24	06.52
(v)	0.4	0.4	0.10	81.98	10.06	07.96
3 (i)	0.4	0.5	0.00	82.75	17.25	00.00
(ii)	0.4	0.5	0.04	81.10	15.12	03.78
(iii)	0.4	0.5	0.06	80.67	13.37	05.96
(iv)	0.4	0.5	0.08	79.95	12.25	07.80
(v)	0.4	0.5	0.10	79.06	11.44	09.50
4 (i)	0.3	0.4	0.00	82.23	17.77	00.00
(ii)	0.3	0.4	0.04	81.37	14.05	04.58
(iii)	0.3	0.4	0.06	81.09	12.26	06.65
(iv)	0.3	0.4	0.08	81.12	10.70	08.18
(v)	0.3	0.4	0.10	80.71	09.01	10.28

The zinc is the most readily deposited metal, under the conditions employed, and the depositions of binary Zn–Ni and ternary Zn–Ni–Co alloys are of anomalous type. This is because the content of zinc (the less noble metal) in the deposit is always higher than its metal ion ratio in the solution [9, 15]. According to previous work [15–17], anomalous codeposition behavior is attributed to the formation of a zinc hydroxide film on the cathode surface due to hydrogen reduction, which suppresses the discharge of nickel and cobalt ions in the deposition of Zn–Ni and Zn–Co alloys.

At zero $CoCl_2$ concentration, as shown in Table 2, the nickel percentage in Zn–Ni alloy deposits increases slightly from 13.07 to 17.77% as the Zn^{2+}/Ni^{2+} molar ratio decreases from 0.5/0.4 to 0.3/0.4. With addition of cobalt chloride, the nickel content in the deposit generally decreases, and reaches 9.01% when the bath contains 0.3/0.4 of Zn^{2+}/Ni^{2+} molar ratio with 0.10 M $CoCl_2$. However, the alloy cobalt content increases to reach 10.28%, under the same conditions.

It can also be seen that the cobalt content in the deposit does not increase only with increasing cobalt chloride but also with increasing Ni^{2+}/Zn^{2+} molar ratio. For example, when the bath contains 0.4/0.5, 0.4/0.4 and 0.5/0.4 molar ratio of Ni^{2+}/Zn^{2+} with 0.1 M Co^{2+}, the alloy cobalt content increases from 5.94 to 7.96% and 9.50%. The increase in deposit cobalt content corresponds to the increase Ni^{2+}/Zn^{2+} molar ratio. This may be attributed to the decrease in the cobalt deposition overpotential due to the increasing Ni^{2+}/Zn^{2+} molar ratio in the bath. A similar behaviour of increasing iron content with increasing Ni^{2+}/Zn^{2+} molar ratio was reported by Younan and Oki [17] in their investigation of the electrodeposition of Zn–Ni–Fe alloy.

The appearance of Zn–Ni alloy thin films depends on the nickel percentage in the bath and the presence and absence of additives. The surface appearance of Zn–Ni deposits obtained were dark, grey and dull, while the electrodeposits of Zn–Ni–Co alloy obtained under the same plating conditions were more uniform, brighter and smoother. Bright and smooth surfaces of Zn–Ni–Co electrodeposits can be obtained from baths containing equal Ni^{2+} to Zn^{2+} molar contents or higher with 0.04 to 0.10 M Co^{2+}.

3.2. *Surface microstructure*

The crystal orientation of electrodeposited Zn–Ni and Zn–Ni–Co alloys with different compositions were characterized by means of X-ray diffraction analysis. The identification of the phases of the deposits was obtained from the line profiles of the X-ray reflection plotted as a function of 2θ, as shown in Figures 1 to 3. The value of the angles corresponding to the peaks and the indices of the crystallography planes of the phases identified, are given in Table 3. Only the γ-$Zn_{21}Ni_5$ was found in Zn–Ni electrodeposits containing more than 9% Ni, in earlier investigations [20, 21]. In this work, the electrodeposits of Zn–Ni alloys with 13.07 to 17.77% nickel content was found to form the single γ phase $Zn_{21}Ni_5$ solid solution, which agrees with the Zn–Ni equilibrium diagram as already observed by some authors [8, 22, 23]. Without cobalt codeposition, as shown in Figures 1–3 in case (a), the γ phase showed a preferential (3 3 0) and (4 1 1) crystal orientation as confirmed by previous work [8].

Under the same electrodeposition conditions, the X-ray diffraction predominance of γ-$Zn_{21}Ni_5$ phases, and the inclusion of the ε-$Zn(OH)_2$ phase, are observed in all the various Zn–Ni–Co deposits compositions obtained in this work. From Figure 1, as example for Zn–Ni–Co electrodeposits, it can be seen that the γ phase of $Zn_{21}Ni_5$ showed an increasing preferred crystal orientation (4 4 2), (6 0 0) and (4 4 4) in comparison with that of (3 3 0) and (4 1 1) with increasing Co content. Also with increasing cobalt alloy content, the intensity of the ε-$Zn(OH)_2$ phase increases in the direction of (0 2 0) crystal orientation. The orientation of the γ phase was due to codeposition of cobalt causing a change in crystal growth of the deposited Zn–Ni alloy. However, the formation of the ε-$Zn(OH)_2$ phase in the alloy may be attributed to hydrogen evolution, which generally increases with increasing cobalt content in the bath (for example, see Table 4). This increase in hydrogen reduction increases the formation of the zinc hydroxide layer at the cathode

Table 3. Crystallographic orientation of zinc–nickel alloy and zinc hydroxide, obtained by X-ray diffraction

Phase	*h k l*	2θ
γ-$Zn_{21}Ni_5$	(3 3 0) (4 1 1)	42.88
	(4 4 2) (6 0 0)	62.38
	(4 4 4)	73.42
ε-$Zn(OH)_2$	(0 2 0)	34.84

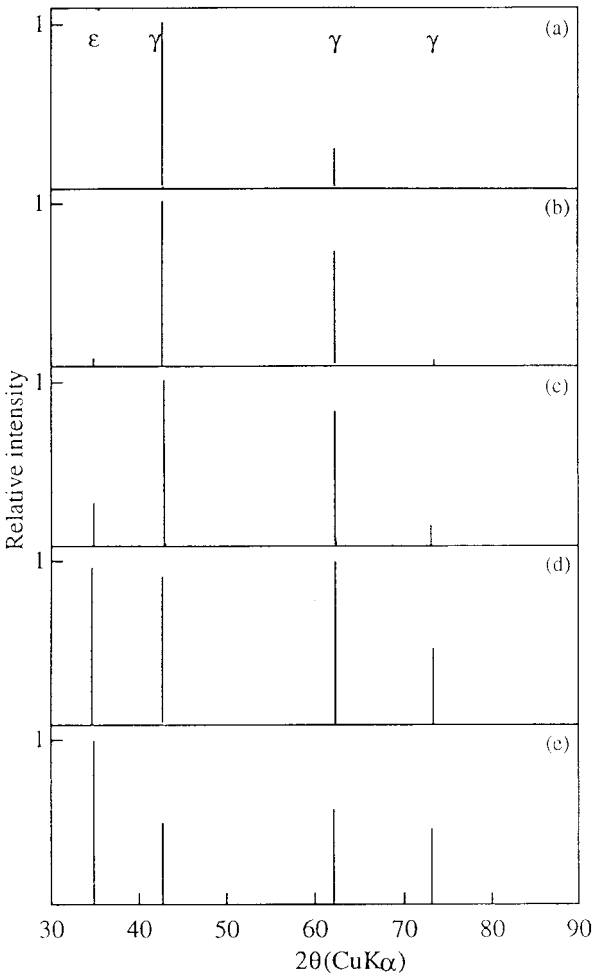

Fig. 1. X-ray diffraction of Zn–Ni–Co electrodeposits having: (a) 13.07%, 0%; (b) 12.48%, 2.24%; (c) 11.93%, 3.88%; (d) 11.23%, 5.24%; and (e) 10.75%, 5.94% of Ni and Co, respectively.

surface [15–17]. The same trend in crystal orientation was observed for different deposits, as shown in Figures 2 and 3.

The change in preferred crystal orientation may be explained by the adsorption inhibition theory [24], some cobalt atoms adsorb on the active planes or sites, which have relative high energy, and inhibit crystal growth at that location. The growth direction of crystals changes due to this inhibition. The remaining plane develops preferred oriented. Through this mechanism, the preferred orientation changes direction.

In these experiments, as there are no organic brighteners in the bath, cobalt acts as inhibitor. The γ-$Zn_{21}Ni_5$ phase grows in the direction of $\langle 4\,4\,2\rangle$, $\langle 6\,0\,0\rangle$ or $\langle 4\,4\,4\rangle$ more than that of $\langle 3\,0\,0\rangle$ or $\langle 4\,1\,1\rangle$ in the baths without cobalt, and the ε-$Zn(OH)_2$ phase grows in the direction $\langle 0\,2\,0\rangle$. As for baths with cobalt, the cobalt adsorbs and codeposits on (4 4 2), (6 0 0) and (4 4 4) and inhibits crystal growth in the direction $\langle 4\,4\,2\rangle$, $\langle 6\,0\,0\rangle$ and $\langle 4\,4\,4\rangle$. Consequently, the relative intensity of (4 1 1), (3 3 0) decreases and that of (4 4 2), (6 0 0), (4 4 4) and (0 2 0) increases with increasing cobalt content up to 5%, approximately, and nickel content (17.77%–12%). Moreover, the highest relative intensity relates to the ε-$Zn(OH)_2$ phase with further increase in cobalt content

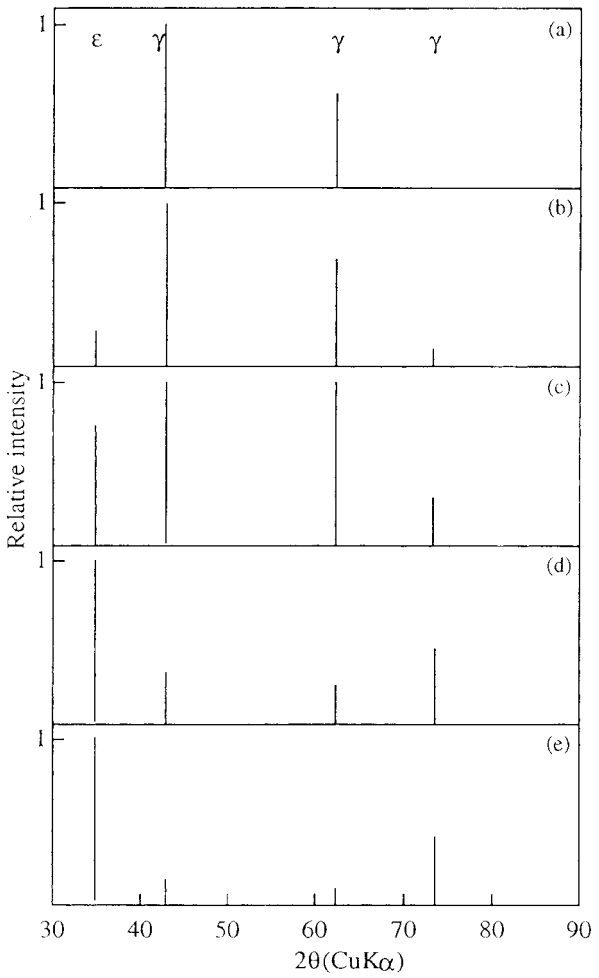

Fig. 2. X-ray diffraction of Zn–Ni–Co electrodeposits having: (a) 15.34%, 0%; (b) 13.78%, 3.26%; (c) 12.37%, 5.16%; (d) 11.24%, 6.52%; and (e) 10.06%, 7.96% of Ni and Co, respectively.

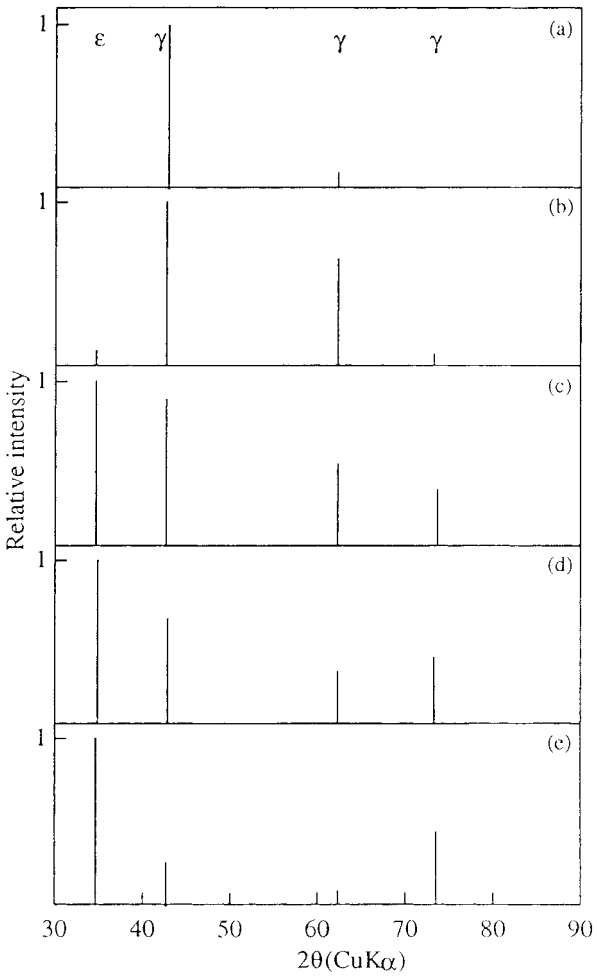

Fig. 3. X-ray diffraction of Zn–Ni–Co electrodeposits having: (a) 17.25%, 0%; (b) 15.12%, 3.78%; (c) 13.37%, 5.96%; (d) 12.25%, 7.80%; and (e) 11.44%, 9.50% of Ni and Co, respectively.

in the electrodeposited Zn–Ni–Co alloy, as shown in Figures 1 to 3. This may be attributed to an increase in hydrogen evolution, which corresponds to the increase in cobalt content in the coating.

Concomitant changes in the structure can be observed from the SEM analysis. Figures 4 to 6 show the surface topography of different electrodeposits. The Zn–Ni deposits showed a homogenous structure with columnar growth of pyramidal form; these grain sizes are fine with increasing nickel content from 15.34% to 17.25%, as shown in Figures 4 and 5, respectively. However, with cobalt codeposition, the ternary Zn–Ni–Co deposits show a more homogenous structure form of crystallites, and the grain size is finer in contrast to that of Zn–Ni deposits, as shown in Figure 6. Moreover, it is found that the grain size decreased with increasing cobalt content in the ternary Zn–Ni–Co deposits, even though the nickel content in these deposits is lower than that of binary Zn–Ni alloy.

3.3. *Corrosion resistance*

The corrosion resistance of Zn–Ni electrodeposits has been studied from an electrochemical standpoint by Kurachi et al. [25]. They measured the corrosion potentials over the full range of Zn–Ni alloy compositions prepared from a sulfate bath. Their results showed that the corrosion potentials become more negative with increasing alloy zinc content. The corrosion resistance of the electrodeposited Zn–Ni alloy was also studied [25–27]; it was concluded that the best corrosion resistance was obtained from deposits containing 11–18% nickel, because these gave the single γ phase alloy.

In the present work, the corrosion resistance of the deposits was evaluated by measuring the anodic current density with overpotential. Figures 7 and 8 show the

Table 4. Effect of metal ion concentration on the alloy cathodic current efficiency

Run	Metals ion concentration/M			Cathodic current efficiency/%
	Zn^{2+}	Ni^{2+}	Co^{2+}	
1	0.4	0.4	0.00	86.22
2	0.4	0.4	0.04	80.80
3	0.4	0.4	0.06	77.50
4	0.4	0.4	0.08	74.90
5	0.4	0.4	0.10	72.88

Fig. 4. SEM micrograph for Zn–Ni alloy deposit with 15.34% nickel content.

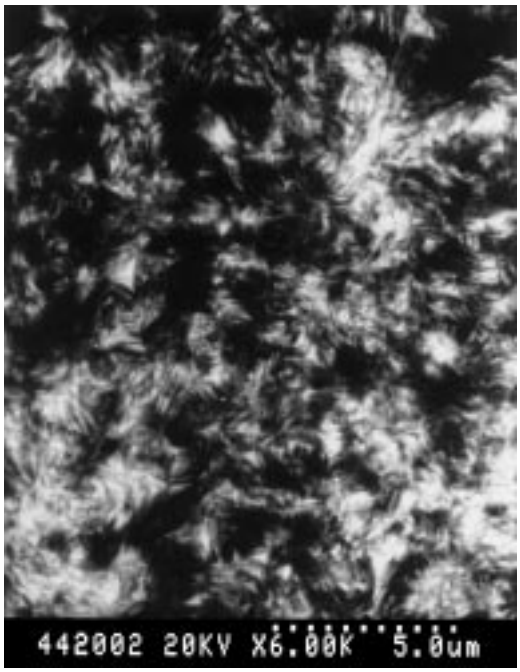

Fig. 6. SEM micrograph for Zn–Ni–Co alloy deposit with 13.79% and 3.26% of nickel and cobalt contents, respectively.

potentiodynamic polarization data of different Zn–Ni and Zn–Ni–Co alloy compositions in 3% neutral sodium chloride electrolyte. It can be seen that, with increasing nickel content, the passive range of the Zn–Ni deposits increases, as shown in curve (1) of Figures 7 and 8.

Under the same plating conditions, it is found that both the rest potential and the passive range of Zn–Ni–Co deposits is generally higher, in contrast to those of Zn–Ni thin films (Table 5 and Figures 7 and 8). For example, Figure 7 shows the potentiodynamic curves of the deposits as a function of cobalt and nickel contents. It can be seen that the passive range of Zn–Ni–Co alloys (curves 2–5) is higher compared with that of the Zn–Ni alloy (curve 1). The passive range of ternary deposits increases with increasing alloy cobalt content up to approximately 6.5%, even in cases of decreasing or equal alloy nickel content, as shown in Figures 7 and 8, respectively.

For the Zn–Ni–Co deposits, the passive range extended from the open circuit potential to about −750 mV, and the anodic current density (at −750 mV) was 0.005 mA cm^{-2} (curve 4 in Figure 7). On the other hand, the passive range of the Zn–Ni deposit extended

Fig. 5. SEM micrograph for Zn–Ni alloy deposit with 17.25% nickel content.

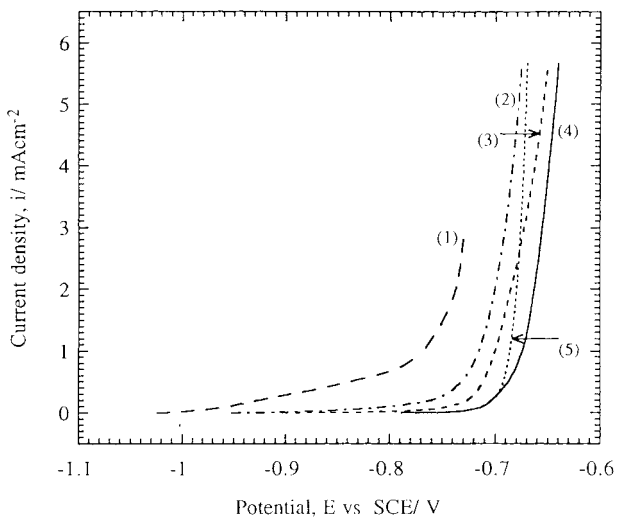

Fig. 7. Anodic polarization curves in neutral 3% NaCl solution, of Zn–Ni–Co electrodeposits having: (1) 15.34%, 0%; (2) 13.78%, 3.26%; (3) 12.37%, 5.16%; (4) 11.24%, 6.52%; and (5) 10.06%; 7.96% of Ni and Co, respectively.

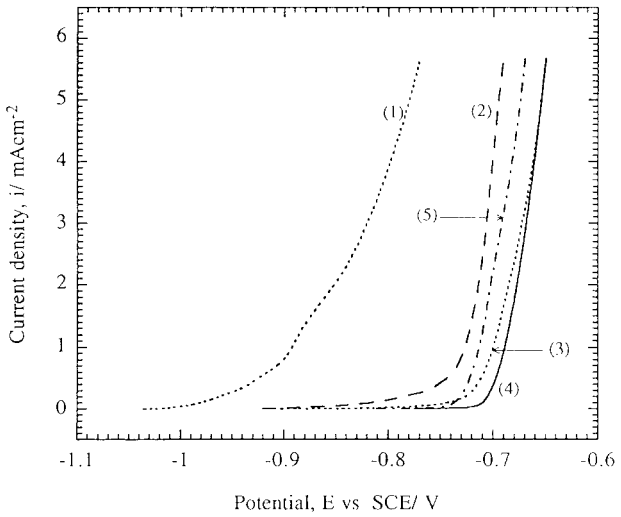

Fig. 8. Anodic polarization curves in neutral 3% NaCl solution, of Zn–Ni–Co electrodeposits having: (1) 13.07%, 0%; (2) 12.48%, 2.24%; (3) 12.37%, 5.16%; (4) 11.26%, 6.65%; and (5) 12.25%, 7.80% of Ni and Co, respectively.

Table 5. Rest potential of electrodeposited alloys in 3% NaCl solution against SCE

Run	Alloy type	Deposit composition/%		Rest potential /–V
		Ni	Co	
1 (i)	Zn–Ni	15.34	00.00	1.024
(ii)	Zn–Ni–Co	13.78	03.26	0.952
(iii)	Zn–Ni–Co	12.37	05.16	0.903
(iv)	Zn–Ni–Co	11.24	06.52	0.789
(v)	Zn–Ni–Co	10.06	07.96	0.771
2 (i)	Zn–Ni	13.07	00.00	1.036
(ii)	Zn–Ni–Co	12.48	02.24	0.921
(iii)	Zn–Ni–Co	12.37	05.16	0.903
(iv)	Zn–Ni–Co	11.26	06.65	0.775
(v)	Zn–Ni–Co	12.25	07.80	0.811

from the open circuit potential to about −950 mV, and the anodic current density (at −950 mV) was 0.113 mA cm^{-2} (curve 1 in Figure 7).

The increase in corrosion resistance of the ternary Zn–Ni–Co deposits is not only due to the formation of a high nickel γ-alloy phase, but also to codeposition of cobalt, which causes a clear change in crystal orientation. Cobalt codeposition in the alloy also tends to produce a finer grain size, as observed by SEM.

4. Conclusion

The electrodeposition of Zn–Ni–Co exhibited anomalous codeposition phenomena. Bright and smooth Zn–Ni–Co alloy surfaces were produced from baths containing equal Ni^{2+} to Zn^{2+} molar contents or higher with from 0.04 to 0.1 M Co^{2+}, even without organic brighteners.

Zn–Ni alloys with 13.07 to 17.77% nickel contents formed the single γ phase of $Zn_{21}Ni_5$ solid solution, with preferred (3 3 0) and (4 1 1) crystal orientation. However, in Zn–Ni Co alloys, the γ phase showed an increasing preferred crystal orientation (4 4 2), (6 0 0) and (4 4 4) with increasing deposit cobalt content, and the inclusion of the ε-$Zn(OH)_2$ phase was also observed in these ternary deposits with preferred (0 2 0) crystal orientation. The ternary Zn–Ni–Co deposits also showed finer grain sizes, in contrast to those of Zn–Ni alloys.

In general, the ternary Zn–Ni–Co deposits showed higher corrosion resistance in comparison with Zn–Ni deposits. The best corrosion resistance was observed for ternary deposits having 11.24% Ni and 6.52% Co. The increase in corrosion resistance of Zn–Ni–Co deposits is not only due to the formation of a high nickel γ-alloy phase but also due to codeposition of cobalt, which causes a clear change in crystal orientation and produces a finer grain size.

References

1. A. Catanzaro, G. Arrigoni, M. Palladino and M. Sarracino, SAE Technical Paper 820583, Detroit, MI (1983).
2. T. Adaniya, M. Omura, K. Matsudo and H. Naemura, *Plat. Surf. Finish.* **68** (1981) 96.
3. A. Shibya, T. Kurimoto, K. Korekawa and K. Noji, *Tetsu to Hagane* **66** (1980) 771.
4. K. Higashi, H. Fukushima, T. Urakawa, T. Adaniya and T. Matsudo, *J. Electrochem. Soc.* **128** (1981) 2081.
5. T. Watanabe, M. Ohmura, T. Honma and T. Adaniya, SAE Technical Paper 820424, Detroit, MI (1982).
6. V. Raman, M. Pushpavanam, S. Jayakishnan and B.A. Shenoi, *Metal Finish.* **81** (1983) 85.
7. G.F. Hsu, *Plat. Surf. Finish.* **71** (1983) 52.
8. R. Noumi, H. Nagasaki, Y. Foboh and A. Shibuya, SAE Technical Paper 820332, Detroit, MI (1982).
9. D.E. Hall, *Plat. Surf. Finish.* **71** (1983) 59.
10. J.A. Dini and H.R. Johnson, *Metal Finish.* **77** (1979) 53.
11. R. Albalat, E. Gomez, C. Muller, M. Sarret, E. Valles and J. Pregonas, *J. Appl. Electrochem.* **20** (1990) 635.
12. T. Tsuda and T. Kurimoto, *US Patent 4 249 999* (10 Feb. 1981).
13. S. Swathirajan, *J. Electrochem. Soc.* **133** (1986) 671.
14. S. Swathirajan, *J. Electroanal. Chem.* **221** (1987) 211.
15. A. Brenner, Electrodeposition of Alloys, Vols. 1 and 2 (Academic Press, New York/London, 1963).
16. F. Elkhatabi, M. Sarret and C. Muller, *J. Electroanal. Chem.* **404** (1996) 45.
17. M.M. Younan and T. Oki, *J. Appl. Electrochem.* **26** (1996) 537.
18. M.M. Younan, R. Ichino and T. Oki, *Metal Finish.* **94** (1996) 46.
19. T. Oki and M.M. Younan, *Galvanotechnik* **87** (1996) 1131.
20. L. Felloni, R. Fratesi and G. Roventi, *J. Appl. Electrochem.* **17** (1987) 574.
21. L. Felloni, R. Fratesi, E. Quadrini and G. Roventi, Proceedings of XXII International Congress, Bologna, Italy (17–19 May 1988), p. 689.
22. T.L. Rama Char and S.K. Panikker, *Electroplat. & Metal Finish.* **13** (1960) 405.
23. M.R. Lambert, R.G. Hart and H.E. Townsed, SAE Technical Paper 831817, Detroit, MI (1983).
24. D.D. Wang and T. Oki, *J. Vac. Sci. Technol., A Vac. Surf. Films* **8** (1990) 3163.
25. M. Kurach, K. Fujiwara and T. Tenaka, Proceeding of Union Electrodeposition Surface Finishing International Congress, N. IbI (Ed.), (1973), p. 152.
26. T.K. Christman, J.H. Payer and L.E. Vaaler, ILZRO Research Report, ZE 286, New York, (1980).
27. D.H. Schantz, *US Patent 2 419 231* (22 Apr 1947).